

Molecular jet study of solvation of pyrazine by small hydrocarbons

J. Wanna and E. R. Bernstein

Citation: *The Journal of Chemical Physics* **84**, 927 (1986); doi: 10.1063/1.450844

View online: <http://dx.doi.org/10.1063/1.450844>

View Table of Contents: <http://aip.scitation.org/toc/jcp/84/2>

Published by the *American Institute of Physics*

**COMPLETELY
REDESIGNED!**



**PHYSICS
TODAY**

Physics Today Buyer's Guide
Search with a purpose.

Molecular jet study of solvation of pyrazine by small hydrocarbons^{a)}

J. Wanna and E. R. Bernstein

Department of Chemistry, Condensed Matter Sciences Laboratory, Colorado State University, Fort Collins, Colorado 80523

(Received 28 March 1985; accepted 3 October 1985)

Supersonic molecular jet 2-color time-of-flight mass spectroscopy studies are reported for pyrazine solvated by methane, ethane, and propane. The results parallel those obtained for benzene and toluene solvated by these molecules. The presence of nitrogen atoms and lone pair electrons in the aromatic system has only a small effect on the cluster structure. Lennard-Jones potential calculations are presented along with the experimental data. Cluster shifts and binding energies are reported and correlated with geometries. The nucleation process for cluster formation appears to involve solvent dimers, as was found for the aromatic hydrocarbon systems.

I. INTRODUCTION

Solvation of aromatic molecules by simple hydrocarbons can be readily explored by supersonic molecular jet spectroscopy. The study reported in this paper expands the range of systems investigated to *N*-heterocyclic aromatic molecules.

We have recently reported several studies of van der Waals (vdW) clusters in which cluster geometry, binding energies, and the cluster nucleation processes have been elucidated.¹⁻⁶ The data in these instances were obtained using fluorescence excitation (FE), dispersed emission (DE), and two-color time-of-flight mass spectroscopy (2-color TOFMS). Coupled with the spectra, potential energy calculations using atom-atom potentials of the exponential-six (exp-6) or Lennard-Jones (LJ) form can provide further detailed insight into cluster geometries and binding energies.⁷ The calculations provide information that complements the spectroscopic data and aids in the identification of stable geometries and in the evaluation of potential energy surfaces. The constants employed in these atom-atom potential calculations are obtained through independent, published parameters that are not fit to our spectroscopic results. The calculations thereby serve as a discrete data set which can be used to verify the experimental conclusions.

Our previous cluster studies have dealt with benzene, toluene, aniline, and *n*-propyl benzene solvated by the simple hydrocarbons methane, ethane, and propane. Significant progress has been made toward a full understanding of these systems¹⁻⁶ in terms of binding energies, relaxation dynamics, and geometries. Two new directions are now being pursued for the extension of these cluster studies: the study of clusters of the above aromatics with hydrogen bonding solvents (i.e., H₂O and NH₃) and the study of heterocyclic aromatic solutes closely related to biologically relevant systems (i.e., DNA bases and amino acids).

Pyrazine (C₄H₄N₂) is chosen as the first solute system to be investigated with these future directions in mind. Pyrazine excitation spectra in the *n*→*π** transition region (~3300 Å) are well known⁸ and thus the study of pyrazine solvation⁹ becomes readily accessible.

Pyrazine clusters with these hydrocarbon solvents are in most respects similar to the benzene hydrocarbon clusters, although subtle differences in geometry due to the nitrogen atoms are found. The LJ potential is employed for the calculations because many independent atom-atom parameters are reported for it; moreover, even specific hydrogen bonding interactions can be incorporated into the calculations as appropriate, through the LJ potential in the 10-12 form.¹⁰

II. EXPERIMENTAL PROCEDURES

The experimental procedures employed in this research are similar to those reported earlier.¹⁻⁶ Two separate lasers are used to generate the ions for 2-color TOFMS: the output of the first laser is scanned through the *n*→*π** pyrazine absorption and the output of the second laser provides the ionization photon, taking the pyrazine from the ¹B_{3u} state to the positive ion, C₄H₄N₂⁺. The pump laser consists of a Nd³⁺/YAG laser pumping a DCM dye laser (~648 nm) whose output is frequency doubled. The ionization laser is of the same configuration but the dye laser operates with R610 dye; the frequency doubled output from the dye laser is further mixed with 1.064 μm from the Nd³⁺/YAG fundamental (~227.3 nm).

The apparatus consists of two chambers separated by a skimmer and a 2 in. gate valve with the (pulsed or cw) nozzle in the first chamber and the mass spectrometer in the second chamber. In this configuration, pyrazine signals are weak due to the relatively low (~12 Torr @ 300 K) vapor pressure of pyrazine. A new pulsed valve, identical in design, operating characteristics, and operating conditions, mounted in the second chamber, is used for these experiments. The mass spectrometer ionization region and flight tube are separated from the nozzle by a skimmer; the distance between the nozzle and the ionization point is about 5 cm. The new configuration increases the signal strength by almost a factor of 10.

Special attention must be given to fragmentation processes in these experiments. If the ionization energy is too large, the solute-solvent clusters fragment and the mass selective information in the experiment is lost. The pyrazine ionization threshold is ~44 000 cm⁻¹ above the ¹B_{3u} first excited singlet state. If as little as 1000 cm⁻¹ more energy is employed to ionize the clusters, significant amounts of fragmentation obscure and interfere with the desired signal.

^{a)}Supported in part by grants from the ARO-D and ONR.

TABLE I. Parameters for the energy expression in the computer modeling.

		$E_{ij} = 1.16 \times 10^5 q_i q_j / 2r_{ij} + A_{ij}/r_{ij}^{12} - C_{ij}/r_{ij}^6$	
		A (cm ⁻¹ Å ¹² /mol)	C (cm ⁻¹ Å ⁶ /mol)
Aliphatic-aliphatic			
C-C		3.168×10^8	1.295×10^5
C-H		4.182×10^7	4.397×10^4
H-H		4.926×10^6	1.591×10^4
Aliphatic-aromatic			
C-C		2.711×10^8	1.517×10^5
C-H		4.217×10^7	4.397×10^4
H-H		4.979×10^6	1.590×10^4
C-N		2.077×10^8	1.348×10^5
H-N		2.500×10^7	4.527×10^4
Aromatic-aromatic			
C-C		2.285×10^8	1.781×10^5
C-H		3.462×10^7	5.217×10^4
H-H		5.028×10^6	1.591×10^4
C-N		1.728×10^8	1.575×10^5
H-N		2.523×10^7	4.527×10^4
N-N		1.312×10^8	1.403×10^5
Aromatic-aliphatic			
C-H		3.431×10^7	5.217×10^4
CH₄:			
	C	-0.08	
	H	0.02	
C₂H₆:			
	C	-0.075	
	H	0.025	
C₃H₈:			
	C	-0.056	
	H	0.021	
C₄H₄N₂:			
	C	0.091	
	H	0	
	N	-0.182	
C₆H₆:			
	C	-0.0074	
	H	$+0.0074$	

Thus, signals from fragmented C₄H₄N₂(CH₄)₂ and C₄H₄N₂(CH₄)₃ can appear in the C₄H₄N₂(CH₄)₁ mass channel at intensities comparable to the C₄H₄N₂(CH₄)₁ signal itself. Fragmentation is not so serious a problem for the other cluster systems we have studied.^{1,2,4-6} In these studies, the ionization energy for all clusters is kept well below 44 000 cm⁻¹.

In conjunction with the experiments, computer calculations are performed using an exp-6 or LJ potential energy function. These calculations give stable cluster geometries, binding energies and barriers to internal cluster motion. The potential form employed for these calculations is

$$E_{ij} \text{ (cm}^{-1}\text{)} = \sum_{i=1}^n \sum_{j=1}^m \left[1.16 \times 10^5 \frac{q_i q_j}{D r_{ij}} + \frac{A^{kl}}{r_{ij}^{12}} - \frac{C^{kl}}{r_{ij}^6} \right], \quad (1)$$

in which the first term constitutes the pairwise electrostatic contribution obtained from interaction between atom *i* and *j* of different molecules, *q_i* and *q_j* are partial electronic charges (in electronic units) centered on each atom, and 1.16×10^5 is a conversion factor to give *E* in cm⁻¹ if *r_{ij}* (the distance between atoms *i* and *j*) is in angstroms. *D* is an effective dielectric constant taken to be 2 in all cases.¹⁰ The sec-

ond and third terms in Eq. (1) constitute the repulsive and attractive van der Waals interaction, respectively, and *k* and *l* refer to different types of atoms. The constants employed in this calculation are given in Table I along with aromatic-aromatic atomic interaction parameters for completeness.

A hydrogen bonding interaction term utilizing a 10-12 potential replaces the 6-12 term in Eq. (1) whenever a hydrogen bonding interaction is encountered. Specifically,

$$E_{HB} = \sum_{i=1}^n \sum_{j=1}^m \left(\frac{A'}{r_{ij}^{12}} - \frac{B}{r_{ij}^{10}} \right), \quad (2)$$

in which the sum over *i* is taken only over the hydrogen bonding atoms H(N), H(O), O, or N in the first molecule and the sum over *j* is taken over the other partner atom in the hydrogen bond belonging to the second molecule. *A'* and *B* constants depend on the type of hydrogen bond formed, in the sense that they depend on the nature of the three atoms involved.¹⁰ In subsequent reports we will use Eq. (2) in the calculation of the binding energy and geometry of the pyrazine dimer, pyrazine ammonia clusters, and pyrazine water clusters.

For comparison purposes, calculations are reported for both LJ and exp-6 potential forms on benzene-methane and benzene-ethane clusters. The calculated binding energies for benzene-methane using these two potentials are 540 and 589 cm⁻¹, respectively. The binding energy is smaller for the LJ

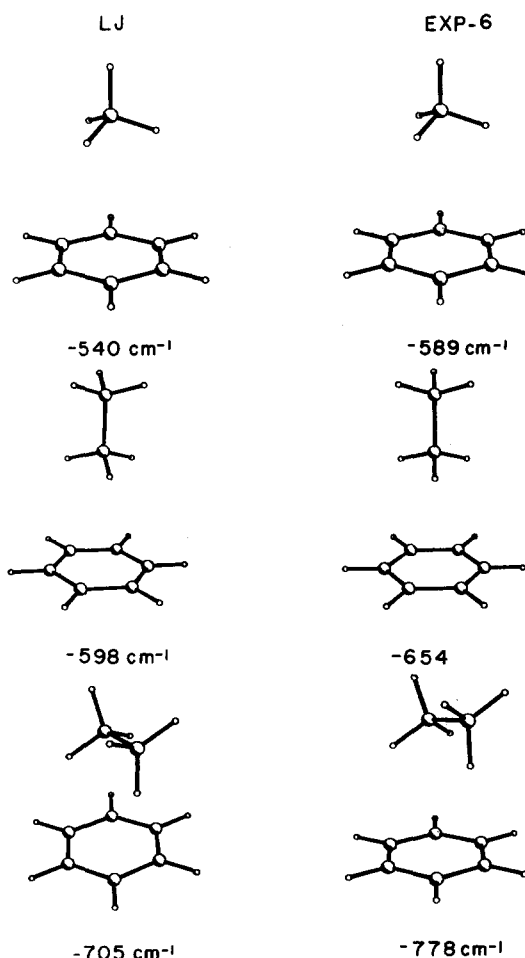


FIG. 1. Comparison of the geometries and binding energies of C₆H₆(CH₄) and C₆H₆(C₂H₆) clusters, based on calculation using Lennard-Jones (LJ) and exponential-6 (exp-6) potentials.

potential than for the exp-6 potential by $\sim 50 \text{ cm}^{-1}$ but the geometries are virtually identical ($\pm 0.05 \text{ \AA}$). Similar findings are obtained for the benzene-ethane clusters: two geometries are predicted using either potential¹ with binding energies for the LJ potential about 50 cm^{-1} below those for the exp-6 potential.¹ Figure 1 displays the computer drawings of these configurations for the different potentials. These two potentials give indistinguishable results for binding energies and geometry estimates to within the experimental accuracy. In all other respects the calculations are carried out as previously reported.

III. RESULTS

2-color TOFMS and FE data are reported below for pyrazine and pyrazine clustered with C_nH_{2n+2} for $n = 1, 2, 3$. Clusters containing up to three solvent molecules are identified and characterized. For each cluster both 0_0^0 and higher vibronic transitions ($6a_0^1$, $10a_0^1$, $10a_0^2$) are observed: experimental data and potential energy calculations will be presented for the various clusters formed.

A. Pyrazine

The singlet $n \rightarrow \pi^*$ transition of pyrazine ${}^1B_{3u} \leftarrow {}^1A_g$ appears at $30\,875.5 \text{ cm}^{-1}$. The $10a_1^1$, $6a_1^1$, and $10a_2^2$ states appear at 383 , 583.7 , and 823 cm^{-1} above the 0_0^0 transition, respectively. The pyrazine spectrum (Fig. 2) is identical in FE or 2-color TOFMS and is the same as has been previously published. The pyrazine structure used in the calculations is obtained from Ref. 11.

B. Pyrazine-methane

The origin of the $C_4H_4N_2(CH_4)_1$ cluster is shifted -33 cm^{-1} from the pyrazine 0_0^0 as shown in Table II and Fig. 3. No vdW modes are observed built on this origin. 2-color TOFMS signals are observed for the $10a_0^1$ and $6a_0^1$ transition but not for the $10a_0^2$ transition of $C_4H_4N_2(CH_4)_1$. Thus, the binding energy for the cluster is between 584 and 823 cm^{-1} .

Based on comparison with other aromatic-hydrocarbon clusters¹⁻⁶ and on potential energy calculations, the minimum cluster energy is associated with the methane molecule coordinated to the π system of the aromatic ring. Figure 4 gives a picture of the CH_4 above the pyrazine plane. The calculated binding energy is 512 cm^{-1} . We expect the

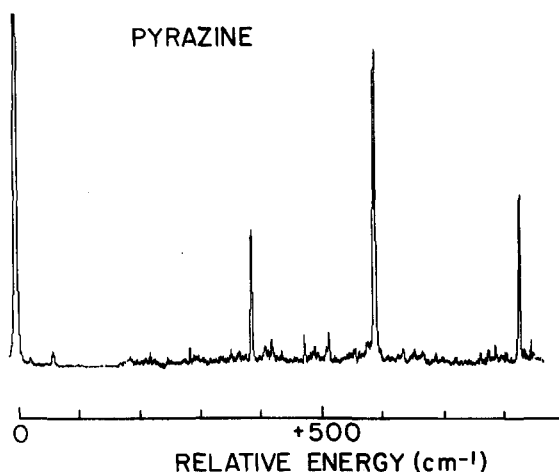


FIG. 2. Time-of-flight mass spectrum (TOFMS) of pyrazine, with the energy scale relative to the 0_0^0 transition ($30\,875.5 \text{ cm}^{-1}$). The three main peaks to higher energy are $10a_0^1$, $6a_0^1$, and $10a_0^2$ at 383 , 584 , and 823 cm^{-1} , respectively.

LJ potential to give somewhat lower than experimental binding energies, as presented above for the benzene test case.

The $C_4H_4N_2(CH_4)_2$ 0_0^0 spectrum displays two peaks, one with a -67.9 cm^{-1} shift and the other with a -39.1 cm^{-1} shift. These data are presented in Fig. 3 and Table II. The larger of the two shifts is nearly twice that observed in the $C_4H_4N_2(CH_4)_1$ cluster: the implication is that the second methane is added symmetrically to the other side of the $C_4H_4N_2(CH_4)_1$ aromatic plane. The -39.1 cm^{-1} shift must then be associated with the (anisotropic) cluster with both methanes on the same side of the aromatic π system.

The LJ calculation of the binding energies and stable geometries for the $C_4H_4N_2(CH_4)_2$ cluster gives results consistent with the above findings. One calculated cluster has methanes on either side of the pyrazine plane in mirror image positions with a binding energy of 1023 cm^{-1} . The second $C_4H_4N_2(CH_4)_2$ configuration features both methanes on the same side of the ring, one shifted toward a nitrogen atom and the other away from the ring; this configuration gives a binding energy of 852 cm^{-1} . Figure 4 shows these geometries.

The $C_4H_4N_2(CH_4)_3$ clusters have more diffuse spectra as is typical for larger clusters. The spectra suggest two config-

TABLE II. Observed peaks in the spectra of pyrazine-methane clusters.

Species	Energy (vac. cm^{-1})	Energy relative to pyrazine 0_0^0 (cm^{-1})	Energy relative to cluster 0_0^0 (cm^{-1})	Assignment ^a
$C_4H_4N_2(CH_4)_1$	30 842.9	-33.1	0	0_0^0
$C_4H_4N_2(CH_4)_2$	30 808.1	-67.9	0	iso 0_0^0
	30 836.9	-39.1	0	aniso 0_0^0
$C_4H_4N_2(CH_4)_3$	30 805.0	-71.0	0	0_0^0
	30 841.0	-35.0	0	0_0^0

^aThe -67.9 cm^{-1} shift is associated with the two methanes added symmetrically above and below the pyrazine ring (isotropic), as shown in Fig. 4. The -39.1 cm^{-1} shift is associated with the anisotropic configuration, as shown in Fig. 4.

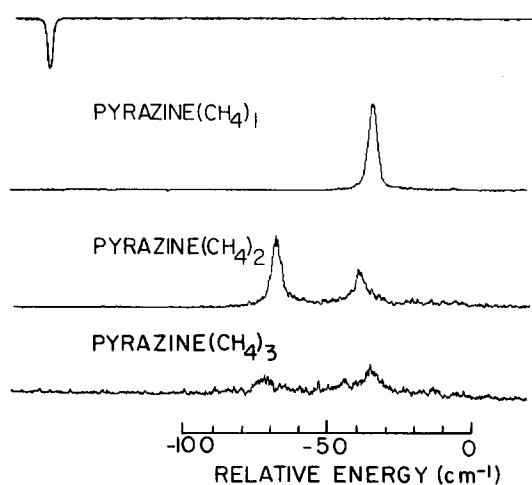


FIG. 3. TOFMS of $C_4H_4N_2(CH_4)_1$, $C_4H_4N_2(CH_4)_2$, and $C_4H_4N_2(CH_4)_3$ in the region of the pyrazine origin. The uppermost trace is the optogalvanic signal used for calibration purposes: on this and the other spectra presented, the feature appears at 6508.3259 \AA (vacuum). The pyrazine origin falls at 0 cm^{-1} on the scale.

urations, one with three methanes on one side of the aromatic plane (-35 cm^{-1}) and one with two methanes on one side and one on the other (-71 cm^{-1}). Figure 3 and Table II give these data.

Calculations were not performed on the $C_4H_4N_2(CH_4)_3$ clusters.

C. Pyrazine-ethane

The 0_0^0 spectrum of $C_4H_4N_2(C_2H_6)_1$ shows three features of roughly equal intensity which can best be attributed to three different geometries (Fig. 5). Two of these features are separated by 4 cm^{-1} and appear at red shifts of 56.3 and 52.5 cm^{-1} . The third feature has a shift of -41.1 cm^{-1} . These are listed in Table III. Some cluster vdW vibronic transitions are also identified (tentatively) to the high energy side of the highest energy $C_4H_4N_2(C_2H_6)_1$ origin. Vibronic transitions are also studied for this cluster and the binding energy can again be bracketed as reported above for $C_4H_4N_2(CH_4)_1$ between $6a^1$ and $10a^2$ per solvent molecule.

The three cluster configurations observed in the spectrum of $C_4H_4N_2(C_2H_6)_1$ are also found in the calculations. These are presented in Fig. 6. The rotational barrier between geometry II and III is 13 cm^{-1} which is probably well above the zero point motion in the ethane rotational coordinate carrying geometry II to III (Fig. 6) by a simple clockwise rotation. Configuration I in Fig. 6 displays the ethane molecule with its long axis nearly coincident with the Z axis of pyrazine ($X = 0.00$, $Y = +0.05 \text{ \AA}$). We have assigned this geometry to the largest of the three cluster shifts because ethane interacts with the π system most strongly in this geometry. This assignment is consistent with the benzene-ethane geometry with the larger cluster shift.¹ The other two geometries find the ethane in asymmetric positions above the ring with the long axis of the ethane more or less parallel to

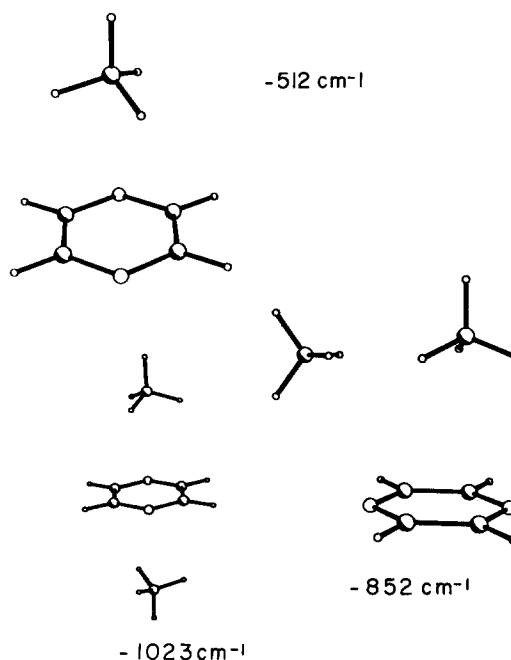


FIG. 4. Minimum energy configurations and binding energies for $C_4H_4N_2(CH_4)_1$ and $C_4H_4N_2(CH_4)_2$ as obtained using a LJ potential calculation.

the plane of the ring. Configuration II has one carbon in ethane situated 3.84 \AA above the C-N bond with the other carbon 3.59 \AA above the ring and pointing towards the diagonally opposite C-N bond. Based on the overall configuration, it would appear as though some "hydrogen bonding" (i.e., hydrogen-nitrogen preferred orientation) is important here, even though a specific hydrogen bonding potential is not employed in the calculation. In the third geometry, configuration III in Fig. 6, the ethane is also in an asymmetric position: here one carbon is 3.81 \AA above C-C bond and the other carbon is 3.56 \AA above the ring pointing towards the other C-C bond. Once again the hydrogens are oriented towards the nitrogen atoms.

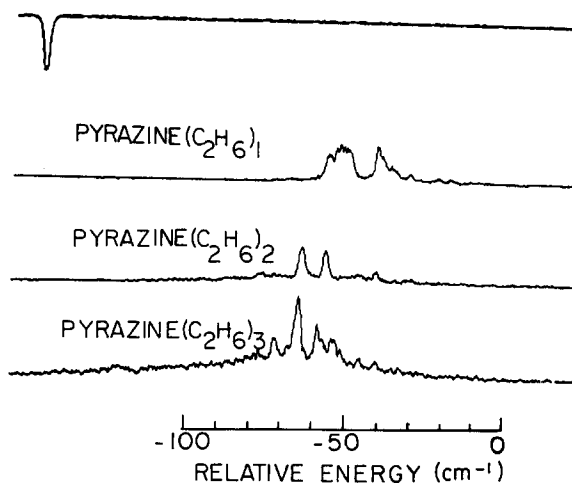


FIG. 5. TOFMS of $C_4H_4N_2(C_2H_6)_1$, $C_4H_4N_2(C_2H_6)_2$, and $C_4H_4N_2(C_2H_6)_3$ in the region of the pyrazine origin (displayed as 0 on the energy scale).

TABLE III. Observed peaks in the spectra of pyrazine-ethane clusters.

Species	Energy (vac. cm^{-1})	Energy relative to pyrazine 0_0^0 (cm^{-1})	Energy relative to cluster 0_0^0 (cm^{-1})	Assignment ^a
$\text{C}_4\text{H}_4\text{N}_2(\text{C}_2\text{H}_6)_1$	30 819.7	- 56.3	0	I 0_0^0
	30 823.5	- 52.5	0	II 0_0^0
	30 834.9	- 41.1	0	III 0_0^0
	30 839.5	- 36.5	16.0	II V_0^1
	30 845.3	- 30.7	10.4	III A_0^1
	30 854.3	- 21.7		
$\text{C}_4\text{H}_4\text{N}_2(\text{C}_2\text{H}_6)_2$	30 811.0	- 65.0	0	II 0_0^0
	30 818.4	- 57.6	0	I 0_0^0
	30 834.2	- 41.8	0	III 0_0^0
$\text{C}_4\text{H}_4\text{N}_2(\text{C}_2\text{H}_6)_3$	30 803.3	- 72.7		
	30 810.5	- 65.5		
	30 816.7	- 59.3		
	30 821.5	- 54.5		
	30 829.9	- 46.1		
	30 835.2	- 40.8		

^a V = a vdW stretch. A = a vdW bend. I, II, III = represents different configurations.

The spectrum of pyrazine with two ethanes shows three features which can be associated with $\text{C}_4\text{H}_4\text{N}_2(\text{C}_2\text{H}_6)_2$ 0_0^0 transitions. Two of these transitions are intense and appear at -65.0 and -57.6 cm^{-1} from the pyrazine 0_0^0 transition. The third feature is identified at -41.8 cm^{-1} from the pyrazine 0_0^0 and is quite weak. The configurations to which we have assigned these features are presented in Fig. 7. Note that none of these features evidences an additive shift with respect to the $\text{C}_4\text{H}_4\text{N}_2(\text{C}_2\text{H}_6)_1$ spectra and thus the isotropic or symmetric $\text{C}_4\text{H}_4\text{N}_2(\text{C}_2\text{H}_6)_2$ configurations are not responsible for the major observed intensity. It is however, possible that the very weak and broad feature at -78 cm^{-1} may be associated with an additive shift cluster.

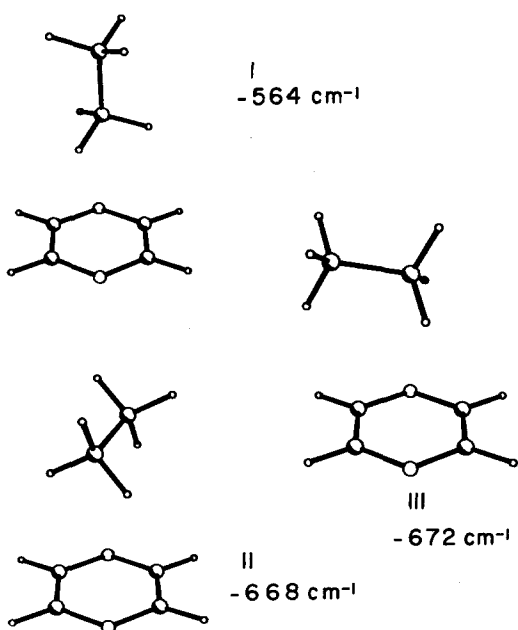


FIG. 6. Minimum energy configurations and binding energies for $\text{C}_4\text{H}_4\text{N}_2(\text{C}_2\text{H}_6)_1$ as obtained using a LJ potential calculation.

Potential energy calculations give four possible low energy asymmetric or anisotropic geometries for the $\text{C}_4\text{H}_4\text{N}_2(\text{C}_2\text{H}_6)_2$ clusters, as depicted in Fig. 7. In each configuration the ethanes are on the same side of the aromatic ring, as mandated by the absence of additive cluster shifts. Two distinctive orientations of the ethanes above the ring are noted. In the first case, configuration I and II, one ethane is perpendicular to and near the center of the aromatic (XY) plane while the other ethane is parallel to the plane and displaced from the ring center. These two geometries are rather similar in binding energy and probably would have similar cluster shifts. The second case (III and IV) has both ethanes parallel to the ring in various positions. The binding energies associated with configurations III and IV (Fig. 7) are also quite similar. Since specific assignments of spectra to geometry can only be made in this instance through comparison with benzene-ethane clusters, we postpone the discussion of such a correspondence until the next section.

Since the major spectra for $\text{C}_4\text{H}_4\text{N}_2(\text{C}_2\text{H}_6)_3$ clusters are found at roughly the same shifts as the spectra for $\text{C}_4\text{H}_4\text{N}_2(\text{C}_2\text{H}_6)_{1,2}$ clusters, we again conclude that the three C_2H_6 molecules are all on the same side of the ring. Note that the base line has now built up under the main features, probably due to the large number of possible configurations for the ethanes not directly coordinated to the pyrazine ring.

D. Pyrazine-propane

The pyrazine-propane system shows results not very different from those presented above and similar to those found for benzene-propane.¹ The spectrum of $\text{C}_4\text{H}_4\text{N}_2(\text{C}_3\text{H}_8)_1$ gives only one peak with a red shift with respect to the pyrazine origin of 60.3 cm^{-1} (see Fig. 8 and Table IV). No other features are observed for this cluster. The calculations associate the spectrum with a geometry in

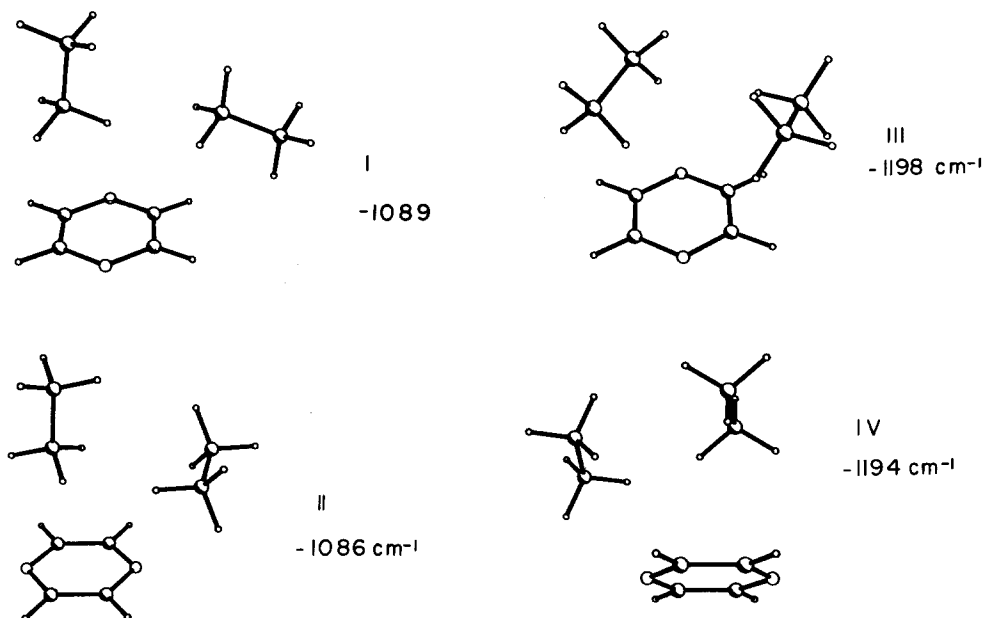


FIG. 7. Minimum energy configurations and binding energies for $C_4H_4N_2(C_2H_6)_2$ as obtained using a LJ potential calculation.

which the propane lies horizontally on the pyrazine ring and roughly 3.7 \AA above it as is depicted in Fig. 9. This configuration has a calculated binding energy of 883 cm^{-1} .

For pyrazine with two propanes we again find no additive shifts and thus conclude both propane molecules are on the same side of the ring. While the spectrum is in general weak, a feature is evident at -102.3 cm^{-1} and two others are clearly observed with smaller shifts (see Fig. 8 and Table IV).

A number of potential energy minima exist for the $C_4H_4N_2(C_3H_8)_2$ system: we have not explored the entire surface for this cluster. One configuration with the propanes arranged as shown in Fig. 9 is stable with a 1012 cm^{-1} bind-

ing energy. Many other configurations are undoubtedly stable for this cluster. Table V gives a list of the calculated and experimental binding energies.

IV. DISCUSSION

The combination of 2-color TOFMS (mass and optical selectivity) and potential energy calculations can be employed to determine cluster geometry and nucleation processes. A comparison between pyrazine-hydrocarbon and benzene-hydrocarbon clusters will be presented in this section along with a brief presentation of the nucleation pro-

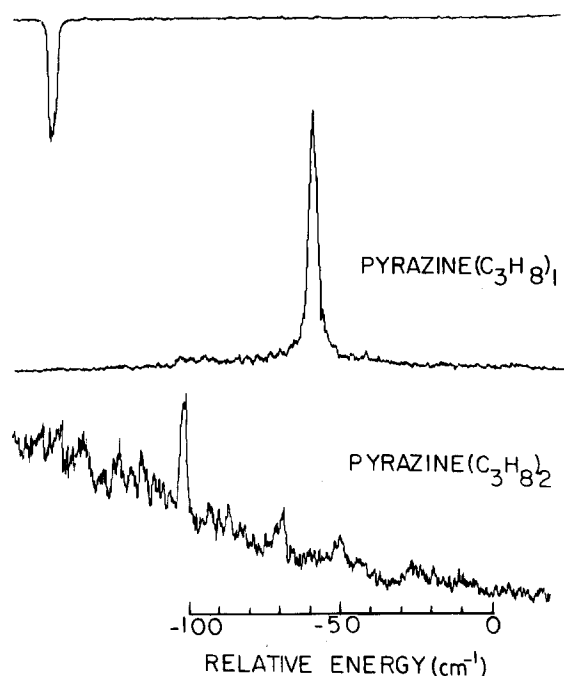


FIG. 8. TOFMS of $C_4H_4N_2(C_3H_8)_1$ and $C_4H_4N_2(C_3H_8)_2$ in the region of pyrazine origin.

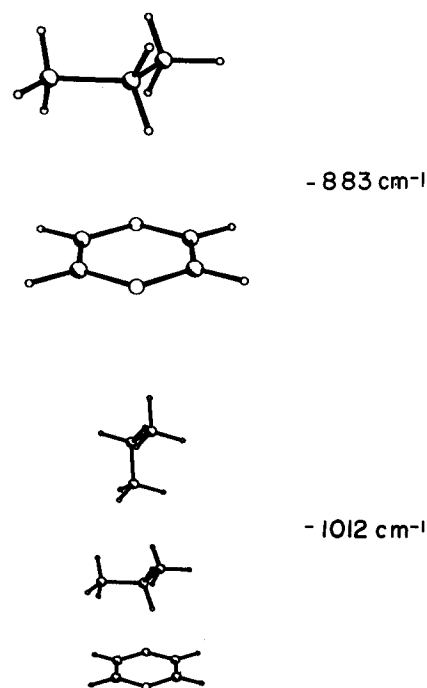


FIG. 9. Minimum energy configuration and binding energies for $C_4H_4N_2(C_3H_8)_1$ and $C_4H_4N_2(C_3H_8)_2$ obtained using a LJ potential calculation.

TABLE IV. Observed peaks in the spectra of pyrazine-propane clusters.

Species	Energy (vac. cm^{-1})	Energy relative to pyrazine 0_0^0 (cm^{-1})	Energy relative to cluster 0_0^0 (cm^{-1})	Assignment ^a
$\text{C}_4\text{H}_4\text{N}_2(\text{C}_3\text{H}_8)_1$	30 815.7	- 60.3	0	0_0^0
$\text{C}_4\text{H}_4\text{N}_1(\text{C}_3\text{H}_8)_2$	30 773.7	- 102.3	0	0_0^0
	30 807.5	- 68.5	0	0_0^0
	30 826.5	- 49.5	0	0_0^0

^a Different possible configurations of $\text{C}_4\text{H}_4\text{N}_2(\text{C}_3\text{H}_8)_2$ give rise to the shifts at - 102.3, - 68.5, and - 49.5 cm^{-1} . See Fig. 9 for an example.

cesses in the beam. Because of the overall similarity between the calculations and data reported in this work and those found in Refs. 1-6 for the benzene, toluene, and aniline clusters, we present a short summary of the major points made in these published papers. The conclusions are as follows:

- (1) Spectral cluster shifts are intimately connected with the geometry of the cluster.
- (2) The size of the shift is governed by the solvent molecule overlap with the aromatic π system of the solute.
- (3) The size of the shift scales with solvent polarizability and the change in solute polarizability upon excitation—hence, the shift is also dependent upon solvent orientation with respect to the solute.
- (4) Additivity of cluster shifts for equivalent structural sites on the solute molecule is maintained to within $\pm 2 \text{ cm}^{-1}$ for benzene, toluene, and aniline solvated by methane, ethane, and propane.
- (5) Calculations of binding energies with the exp-6 atom-atom potential gives binding energies to within the experimental accuracy.

- (6) According to the exp-6, LJ benzene comparison calculation, the calculated LJ binding energy is expected to be $\sim 50 \text{ cm}^{-1}$ below the calculated exp-6 binding energy.
- (7) Both potentials give geometries that are, to within calculational accuracy, identical.
- (8) The calculated geometries agree with the benzene experimental geometries which are uniquely identified based on symmetry consideration.
- (9) In all instances for which comparisons are possible, the calculations agree with the experimental findings and vice versa.

A. Pyrazine-methane

Pyrazine solvated by methane produces a set of $n \rightarrow \pi^*$ spectra that are in general simple to interpret. The $\text{C}_4\text{H}_4\text{N}_2(\text{CH}_4)_1$ complex evidences only one transition for each vibronic feature of pyrazine observed. No vdW mode vibronic additions to the cluster 0_0^0 , $10a^1$, $6a^1$, or $10a^2$ are observed. We attribute the absence of $\Delta\nu = \pm 1$ vibronic

TABLE V. Binding energies for C_6H_6 and $\text{C}_4\text{H}_4\text{N}_2$ with various hydrocarbons.

Species	Configuration	Calculated (cm^{-1})		Experimental (cm^{-1})
		LJ ^a	Exp-6	
$\text{C}_6\text{H}_6(\text{CH}_4)_1$		- 540	- 589	
$\text{C}_6\text{H}_6(\text{C}_2\text{H}_6)_1$	I	- 598	- 654	
$\text{C}_6\text{H}_6(\text{C}_2\text{H}_6)_1$	II	- 705	- 778	
$\text{C}_4\text{H}_4\text{N}_2(\text{CH}_4)_1$		- 512		584 < B.E. < 823
$\text{C}_4\text{H}_4\text{N}_2(\text{CH}_4)_2$	iso	- 1023		
$\text{C}_4\text{H}_4\text{N}_2(\text{CH}_4)_2$	aniso	- 852		
$\text{C}_4\text{H}_4\text{N}_2(\text{C}_2\text{H}_6)_1$	I	- 564		584 < B.E. < 823
$\text{C}_4\text{H}_4\text{N}_2(\text{C}_2\text{H}_6)_1$	II	- 668		
$\text{C}_4\text{H}_4\text{N}_2(\text{C}_2\text{H}_6)_1$	III	- 672		
$\text{C}_4\text{H}_4\text{N}_2(\text{C}_2\text{H}_6)_2$	I	- 1089		
$\text{C}_4\text{H}_4\text{N}_2(\text{C}_2\text{H}_6)_2$	II	- 1086		
$\text{C}_4\text{H}_4\text{N}_2(\text{C}_2\text{H}_6)_2$	III	- 1198		
$\text{C}_4\text{H}_4\text{N}_2(\text{C}_2\text{H}_6)_2$	IV	- 1194		
$\text{C}_4\text{H}_4\text{N}_2(\text{C}_3\text{H}_8)_1$		- 883		
$\text{C}_4\text{H}_4\text{N}_2(\text{C}_3\text{H}_8)_2$		- 1012		

^a The LJ potential gives lower binding energies than the exp-6 potential, although the geometrical configurations calculated with both potentials are identical.

transitions to the similarity of the ground and excited state vdW potential energy surfaces. These surfaces are more nearly identical than those of any other system we have studied.¹⁻⁶ This similarity can be rationalized based on the nature of the electronic transition. In a $\pi \rightarrow \pi^*$ transition, an electron involved in the ground state binding of, for example, benzene and methane is removed from a bonding orbital and placed in an antibonding orbital. However, the $n \rightarrow \pi^*$ transition removes a nonbonding electron, probably not very much involved in the overall pyrazine-methane interaction, and places it in an antibonding orbital again not heavily involved in the cluster bonding. Thus the ground and excited state potential energy surfaces must be nearly superimposable, even though the excited state well is $\sim 40 \text{ cm}^{-1}$ deeper. Moreover, this argument suggests that the $\text{C}_6\text{H}_6(\text{CH}_4)_1$ and $\text{C}_4\text{H}_4\text{N}_2(\text{CH}_4)_1$ clusters should have similar shifts because both ground and excited state π systems are nearly the same. The methane in a pyrazine-methane complex coordinates with the aromatic π system in much the same manner as found for $\text{C}_6\text{H}_6(\text{CH}_4)_1$.

The $\text{C}_4\text{H}_4\text{N}_2(\text{CH}_4)_2$ system is again very similar to the $\text{C}_6\text{H}_6(\text{CH}_4)_2$ system.¹ Both isotropic and anisotropic configurations are observed. The intensity ratio of the isotropic to anisotropic clusters is roughly 2:1, again as found for the benzene system. The second, asymmetric methane does not overlap the ring and thus contributes little to the cluster shift which is nearly the same as found for $\text{C}_4\text{H}_4\text{N}_2(\text{CH}_4)_1$. The binding energy for the symmetric cluster is 1023 cm^{-1} and for the asymmetric cluster is 852 cm^{-1} . $\text{C}_6\text{H}_6(\text{CH}_4)_2$, on the other hand, has both symmetric and asymmetric clusters with nearly the same binding energy (approximately 1180 cm^{-1}).

B. Pyrazine-ethane

The $\text{C}_4\text{H}_4\text{N}_2(\text{C}_2\text{H}_6)_1$ cluster can have three distinct geometrical arrangements with roughly equal probability and similar binding energies (Fig. 6), whereas $\text{C}_6\text{H}_6(\text{C}_2\text{H}_6)_1$ displays only two configurations. This difference must be a direct consequence of the presence of the nitrogen atoms in the aromatic ring. The cluster with the largest spectral shift (-56.3 cm^{-1}) has been assigned as the one for which the ethane is perpendicular to the pyrazine ring. In $\text{C}_6\text{H}_6(\text{C}_2\text{H}_6)_1$ this geometry has a shift of -57.2 cm^{-1} . In both instances this configuration has the smallest binding energy. Weak vibronic $\Delta v = \pm 1$ transitions are observed for the $\text{C}_4\text{H}_4\text{N}_2(\text{C}_2\text{H}_6)_1$ clusters and thus the vdW potentials for the ground and excited states are somewhat different.

We can assign the two parallel orientation clusters to specific shifts (-52.5 and -41.1 cm^{-1}) in the same manner suggested for the aromatic hydrocarbons: the cluster with the larger overlap between the solute π system and the solvent has the larger cluster shift. Thus the geometry (II in Fig. 6) with the C_2H_6 oriented toward the C-N bond is associated with the -52.5 cm^{-1} shift and the geometry with the C_2H_6 oriented toward the C-C bond is associated with the -41.1 cm^{-1} shift. This correlation is at least consistent with all other systems we have studied to date.

Three distinct features are observed for the $\text{C}_4\text{H}_4\text{N}_2(\text{C}_2\text{H}_6)_2$ clusters. Figures 5 and 7 present the spectra

and calculated geometries. Calculated configurations I and II are quite similar, as are calculated configurations III and IV. In either grouping only one ethane is well coordinated with the aromatic ring: in the first set the coordinated ethane is perpendicular to the ring and in the second it is parallel. The nitrogen atoms seem to play a central role in these geometries because for $\text{C}_6\text{H}_6(\text{C}_2\text{H}_6)_2$ the two ethanes are always perpendicular to the ring.

We suggest, based on arguments and correlations made previously,¹ that configuration I and II can be associated with spectral cluster shifts of -57.6 and -65.0 cm^{-1} . Configuration II can be assigned to the -65.0 cm^{-1} feature for two reasons: the perpendicular ethane has slightly more overlap with the ring in this geometry and this geometry has the slightly lower binding energy. The shift at -41.1 cm^{-1} is attributed to the configuration IV since one ethane has an overlap with the ring similar to the $\text{C}_4\text{H}_4\text{N}_2(\text{C}_2\text{H}_6)_1$ case. Configuration III is not readily assigned to any of the observed features.

C. Pyrazine-propane

The geometry in this instance for $\text{C}_4\text{H}_4\text{N}_2(\text{C}_3\text{H}_8)_1$ is very similar to that found for $\text{C}_6\text{H}_6(\text{C}_3\text{H}_8)_1$. Apparently the nitrogen atoms do not affect the orientation of the propane above the pyrazine.

D. Nucleation

Both symmetric (isotropic) and asymmetric (anisotropic) clusters are possible for the solute(solvent)₂ systems. The isotropic clusters have a solvent molecule on either side of the ring and the anisotropic clusters have both solvent molecules on the same side of the ring. Both types of solute-(solvent)₂ clusters can be formed through homogeneous nucleation,^{1,2} the addition of one solvent molecule at a time to the cluster. Inhomogeneous nucleation, the addition of two molecules to the cluster simultaneously, can only produce anisotropic clusters. We have previously shown that the supersonic molecular jet conditions (i.e., backing pressure, nozzle diameter, pumping speed, concentration ratios) used in our laboratory deplete the beam of solvent monomer species.

The $\text{C}_4\text{H}_4\text{N}_2(\text{CH}_4)_2$ cluster spectrum show isotropic and anisotropic clusters in roughly similar amounts. Pyrazine expanded with ethane or propane, on the other hand, gives only anisotropic clusters. These concentration ratios are a consequence of the nucleation processes in the beam as we have demonstrated for benzene and toluene.^{7,8} A complete discussion of these mechanisms can be found in our previous papers.

V. CONCLUSION

Pyrazine-hydrocarbon clusters are in general similar to benzene hydrocarbon clusters: the presence of nitrogen atoms in the aromatic ring has a relatively small although discernable effect on the overall solute-solvent interaction. In particular, solvent hydrogen atoms preferentially orient toward the solute nitrogen atoms. While some minor differ-

ences do exist, the cluster spectral shifts for the two series are quite similar as well.

Calculations of geometries and binding energies using either the LJ or an exp-6 potential produce nearly identical results for benzene and pyrazine species. The results based on either potential form are in agreement with experiments and are self-consistent for all species thus far studied.

Inhomogeneous nucleation predominates as the main process in the formation of solute(solvent)₂ clusters.

¹M. Schauer and E. R. Bernstein, *J. Chem. Phys.* **82**, 726 (1985).

²M. Schauer, K. S. Law, and E. R. Bernstein, *J. Chem. Phys.* **82**, 736 (1985).

³K. S. Law and E. R. Bernstein, *J. Chem. Phys.* **82**, 2856 (1985).

⁴K. S. Law, M. Schauer, and E. R. Bernstein, *J. Chem. Phys.* **81**, 4871 (1984).

⁵E. R. Bernstein, K. Law, and M. Schauer, *J. Chem. Phys.* **80**, 207 (1984).

⁶M. Schauer, K. Law, and E. R. Bernstein, *J. Chem. Phys.* **81**, 49 (1984).

⁷M. J. Ondrechen, Z. Berkovitch-Yellin, and J. Jortner, *J. Am. Chem. Soc.* **103**, 6586 (1981).

⁸E. F. Zalewski, D. S. McClure, and D. L. Narva, *J. Chem. Phys.* **61**, 2964 (1974).

⁹J. Lee, F. Li, and E. R. Bernstein, *J. Phys. Chem.* **87**, 260 (1983).

¹⁰(a) F. A. Momany, L. M. Carruthers, R. F. McGuire, and H. A. Scheraga, *J. Phys. Chem.* **78**, 1595 (1974); (b) G. Nemethy, M. S. Pottle, and H. A. Scheraga, *ibid.* **87**, 1883 (1983).

¹¹P. J. Wheatly, *Acta Crystallogr.* **10**, 182 (1957).